IET Electric Power Applications

Special issue Call for Papers

Be Seen. Be Cited.
Submit your work to a new IET special issue

Connect with researchers and experts in your field and share knowledge.

Be part of the latest research trends, faster.

Read more

IET The Institution of Engineering and Technology

| IET Electric Power Applications

In-depth investigation of inter-turn short-circuit faults of surface-mounted permanent magnet machines with series-parallel coil connections

Zeting Mei[1] | Guang-jin Li[1] [iD] | Zi-Qiang Zhu[1] [iD] | Richard Clark[2] |
Arwyn Thomas[2] | Ziad Azar[2]

[1]Department of Electronic and Electrical Engineering, The University of Sheffield, Sheffield, UK

[2]Siemens Gamesa Renewable Energy Limited, Sheffield, UK

Correspondence

Guang-jin Li.
Email: g.li@sheffield.ac.uk

Funding information

Engineering and Physical Sciences Research Council, Grant/Award Number: EP/R004900/1

Abstract

A general analytical model is developed in a concise block matrix form for surface-mounted permanent magnet (SPM) machines with series-parallel coil connections under inter-turn short circuit (ITSC) fault. In the model, branch currents are used as state variables and inductances of different series-parallel coil connections are calculated using an analytical method, namely winding function approach (WFA) together with slot permeance method. Based on the characteristics of the calculated inductances and the developed fault model, the multiphase Clarke transformation has been proposed to simplify the fault model. In the process of model simplification, the healthy machine model using branch currents as state variables have been proven to be equivalent to that using 3-phase currents as state variables. The proposed fault models of a 3kW 96-slot 32-pole SPM machine with different series-parallel coil connections have been built in Matlab/Simulink and validated by time-stepping 2D FE simulations. Simulation results show that different series-parallel coil connections have little influence on the amplitude of the ITSC current. Finally, a small scale 24-slot 8-pole SPM machine prototype has been built to further validate the accuracy of the proposed fault model.

KEYWORDS

electric machines, fault diagnosis, permanent magnet machines, short-circuit currents

1 | INTRODUCTION

As one of the most promising renewable energy sources, wind power is becoming more and more competitive and attracts increasing attention from industry and academia. Most countries have a strong motivation to transform the way of electricity generation from the conventional energy sources such as natural gas, oil, coal, and nuclear to more eco-friendly energy sources such as solar and wind. It has been reported that since the 1990s, the cumulative capacity of the installed wind energy has increased exponentially. In the near future, both the power capacity and size of a single commercial wind turbine are expected to increase [1]. However, if there is a severe fault in a large wind turbine, it often requires complex and costly

maintenance works [2]. This is particularly the case for offshore wind turbines, which are much more difficult to access to than their onshore counterparts. Therefore, despite many technological advances have been made in recent years, the reliability of wind turbine systems remains a growing concern to both academia and industry. Based on the distribution of number of failures and downtime in different components of a wind turbine recorded by major wind turbine manufacturers [3], it is found that although the failure rate of large wind generators is not the highest, the downtime of which is often one of the longest. This shows the necessity of investigating the faults in large wind generators.

Regarding the faults of large wind generators, one early literature review [4, 5] showed that the winding fault is one of

the most frequent faults, second only to the bearing fault. According to statistical data, it is found that there are five major types of winding faults, namely (1) open circuit of one phase, (2) inter-turn (turn-to-turn) short circuit (ITSC), (3) coil to coil short circuit, (4) phase to phase short circuit, and (5) coil/phase to ground short circuit [6]. And the ITSC fault is often regarded as one of the root causes of other more severe faults [7]. If the ITSC fault can be detected and mitigated in time, the amount of maintenance work could be reduced, and the wind generators will be able to operate more efficiently during their designed life span. Hence, an in-depth investigation of the ITSC faults and their impact on the performance of electrical machines are necessary. This can be done by using the physics-based fault modelling, which has attracted an increasing interest from both the academia and industry in recent years [8–11].

In [10, 11], a general analytical model of surface-mounted permanent magnet (SPM) machines with series-connected and parallel-connected coils under ITSC fault were proposed. However, for medium and large-power electrical machines, such as the ones used in wind power, series-parallel coil connections are often used to increase the phase current whilst reducing the phase voltage level, and the models based on series-connected and parallel-connected coils might no longer be applicable. In [12–14], the transient behaviour of salient-pole synchronous machines with series-parallel coil connections under internal faults including ITSC fault was modelled using branch currents as state variables due to unequal branch currents when an internal fault happens. However, the cumbersome inductance calculation considering the practical distributed winding arrangement and large-scale systems of differential equations required to characterise the fault model make ITSC fault modelling for large salient-pole synchronous generators quite complex and challenging. In addition, the fault models proposed in [12–14] are not really general and simple, and they cannot provide much meaningful physical insights into the fault performance.

In [15], ITSC fault models for fractional-slot SPM machines with series-connected and parallel-connected windings have been developed. To simplify the modelling, the authors have assumed that all branch currents in healthy phases (phases B and C) were equal when the ITSC fault occurred in the faulty phase (phase A) branch. In [16], the same assumption has been made about the branch currents during the ITSC fault when modelling the fractional-slot SPM machines with multi-strand windings. However, both [15, 16] only modelled one specific fractional-slot SPM machine, and their assumptions are not always valid for integer-slot SPM machines with series-parallel coil connections as it will be investigated in this paper.

As for other fault modelling methods such as a magnetic equivalent circuit [17, 18] and finite element analysis (FEA) [19–21], they are quite time-consuming particularly the FEA for large-power electrical machines under the ITSC fault. This is mainly because, due to the large numbers of slots and poles, full FE models required for large-power SPM machines with ITSC faults often have much more mesh elements, and are hence much more time consuming to solve. This is particularly the case when the FE models are coupled with PWM converters (co-simulation) to simulate the faulty machine performance under real operating conditions. In addition, it is noticed that large-power SPM machines need more time to reach a steady state, hence requiring longer simulation time.

Different from the developed fault models in [12–16], this paper proposes a general and relatively simple analytical fault model in a concise block matrix form for SPM machines with series-parallel coil connections using branch currents as state variables. In the fault model, the mutual inductive coupling between any two branches has been considered. It should be mentioned that, as shown in Figure 1, the winding of the analysed SPM machines is single-layer, full-pitch, and distributed [slot/pole/phase (SPP) is equal to 1], which is often the case for large PM generators used in wind power.

Due to this simple winding structure, inductances of the fault model can be calculated easily by analytical methods such as winding function approach (WFA) together with slot permeance method. It is worth noting that the core saturation has been neglected during the analytical calculation of the inductances. Once the inductances are determined, it is found that the multiphase Clarke transformation can be used to simplify the fault model based on the characteristics of the calculated inductances and the concise block matrix form of the developed fault model. As an example, fault models of a 3kW 96-slot 32-pole SPM machine with different series-parallel coil connections, have been built in Matlab/Simulink based on the proposed fault model and model simplification method, and they have been validated by time-stepping 2D FE simulations. In addition, a small scale 24-slot 8-pole SPM machine prototype has been built to further validate the accuracy of the proposed fault model.

2 | MODELLING OF THE ITSC FAULT OF SPM WIND GENERATORS

A schematic representation of series-parallel coil connections of an SPM machine is shown in Figure 2, where the ITSC fault is assumed to be in the first branch (A1 branch) of phase A. Here it is also assumed that one parallel branch has r coils in series, and n parallel branches of one phase will therefore contain $p = r \times n$ coils in total, where p is the number of pole pairs. This is because the windings of the analysed SPM machines are single-layer, integer-slot, and distributed, thus the number of pole pairs p is the same as the number of coils in one phase winding. To simplify the analyses, in the following sections of this paper, rS $\times$ nP will be used to represent the windings with r series coils (in each branch) and n parallel branches (in each phase).

In addition, the short-circuited turns of the A11 faulty coil is named as A11_fm shown in Figure 2. Assuming that the short-circuited turns A11_fm are somewhere in the middle of the affected slots, then A11_ht and A11_hb will represent the remaining healthy turns at the top and at the bottom of the affected slots, respectively. As for A1_hc, it represents the remaining healthy $r - 1$ coils of the A1 branch. Some mutual
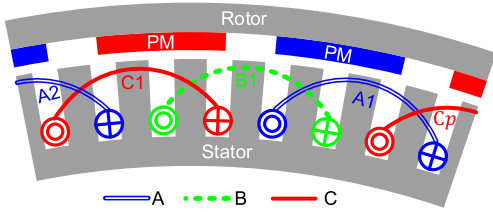
FIGURE 1 The studied surface-mounted permanent magnet (SPM) machine with integer slot overlapping windings.
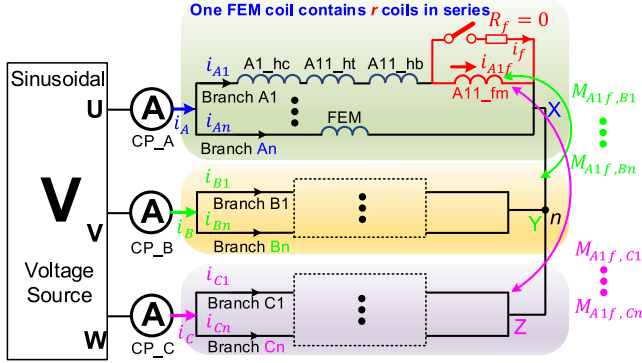

FIGURE 2 Circuit schematic of the studied surface-mounted permanent magnet (SPM) machines under ITSC fault. One FEM coil contains r coils in series, and each phase has n parallel branches.

inductances between the short-circuited turns and the other branches such as $M_{A1f,An}$, $M_{A1f,B1}$, $M_{A1f,Cn}$, etc are also illustrated in Figure 2.

From Figure 2, the voltage equations for every circuit branch can be expressed in a compact matrix form as

$$
\begin{bmatrix} \mathbf{v}_A \\ \mathbf{v}_B \\ \mathbf{v}_C \end{bmatrix} = \begin{bmatrix} \mathbf{L}_{AA} & \mathbf{M}_{AB} & \mathbf{M}_{AC} \\ \mathbf{M}_{BA} & \mathbf{L}_{BB} & \mathbf{M}_{BC} \\ \mathbf{M}_{CA} & \mathbf{M}_{CB} & \mathbf{L}_{CC} \end{bmatrix} \frac{d}{dt} \begin{bmatrix} \mathbf{i}_A \\ \mathbf{i}_B \\ \mathbf{i}_C \end{bmatrix} + R_{cb} \begin{bmatrix} \mathbf{i}_A \\ \mathbf{i}_B \\ \mathbf{i}_C \end{bmatrix}
$$
$$
+ \begin{bmatrix} \mathbf{e}_A \\ \mathbf{e}_B \\ \mathbf{e}_C \end{bmatrix} - \begin{bmatrix} R_{A1f} \\ 0 \\ \vdots \\ 0 \end{bmatrix} i_f - \begin{bmatrix} \mathbf{M}_{Af} \\ \mathbf{M}_{Bf} \\ \mathbf{M}_{Cf} \end{bmatrix} \frac{di_f}{dt}
$$

$$(1)$$

where column vectors **v**, **i**, and **e** represent branch-to-neutral voltages (v), branch back-EMFs, (e) or branch currents (i) for the phases A, B, and C windings. For instance, $\mathbf{v}_A = \begin{bmatrix} v_{A1} & v_{A2} & \cdots & v_{An} \end{bmatrix}^T$, and it has n entries, where n is the number of parallel branches defined earlier. Additionally, i_f is the current in the short-circuit path as shown in Figure 2. As for $\mathbf{L}_{xx}$ and $\mathbf{M}_{xy}$ ("y" represents another phase winding different from x), they are named as branch inductance matrices in this paper. It is worth mentioning that the (i,j)th entry of $\mathbf{L}_{xx}$ represents the inductive coupling between the ith and jth branches of the same phase x. The (i,j)th entry of $\mathbf{M}_{xy}$ represents the inductive coupling between the ith branch of the phase x and the jth branch of the phase y. These

representations can be interpreted as $(\mathbf{L}_{xx})_{i,j} = M_{xixj}$ and $(\mathbf{M}_{xy})_{i,j} = M_{xiyj}$. In addition, R_{cb} in Equation (1) is the branch resistance, and R_{A1f} is the resistance of the short-circuited turns. The elements of three column vectors $\mathbf{M}_{Af}$, $\mathbf{M}_{Bf}$, and $\mathbf{M}_{Cf}$ represent the inductive couplings between the short-circuited turns and the branches in all three phases, and they are given as

$$
\begin{cases}
\mathbf{M}_{Af} = \begin{bmatrix} L_{A1f,A1f} + M_{A1b,A1f} & M_{A2,A1f} & \cdots & M_{An,A1f} \end{bmatrix}^T \\
\mathbf{M}_{Bf} = \begin{bmatrix} M_{B1,A1f} & M_{B2,A1f} & \cdots & M_{Bn,A1f} \end{bmatrix}^T \\
\mathbf{M}_{Cf} = \begin{bmatrix} M_{C1,A1f} & M_{C2,A1f} & \cdots & M_{Cn,A1f} \end{bmatrix}^T
\end{cases}
$$

$$(2)$$

where $L_{A1f,A1f}$ is the self-inductance of the short-circuited turns, and $M_{A1b,A1f}$ represents the mutual inductance between the remaining healthy turns and the short-circuited turns in the branch A1.

The voltage equation of the short-circuited path is

$$
\left(R_f + R_{A1f} \right) i_f + L_{A1f,A1f} \frac{di_f}{dt} - e_{A1f} - R_{A1f} i_{A1}
$$
$$
= \left(\mathbf{M}_{Af} \right)^T \frac{d\mathbf{i}_A}{dt} + \left(\mathbf{M}_{Bf} \right)^T \frac{d\mathbf{i}_B}{dt} + \left(\mathbf{M}_{Cf} \right)^T \frac{d\mathbf{i}_C}{dt}
$$

$$(3)$$

where R_f is the contact or insulation resistance between two short-circuited points. In the following sections about the simulations of the 3kW SPM machine, R_f is assumed to be zero to simplify the analyses. $e_{A1f} = (\mu_1/r)e_A$ is the back EMF of the short-circuited turns, where the coil faulty turn ratio μ_1 is defined as $\mu_1 = n_f/n_c$ for the studied integer-slot SPM machines and e_A is the branch back EMF of phase A. In addition, n_f is the number of short-circuited turns A11_fm and n_c indicates the number of turns per coil.

For a wye-connected 3-phase windings having series-parallel coil connections, the branch currents need to obey Kirchhoff's current law such as

$$
\sum_{k=1}^{n} i_{Ak} + \sum_{k=1}^{n} i_{Bk} + \sum_{k=1}^{n} i_{Ck} = 0
$$

$$(4)$$

Additionally, if there are space harmonics in the branch back EMFs in Equation (1) and the neutral point is not accessible, then the three branch-to-neutral (or phase) voltages v_A, v_B, and v_C cannot be determined directly from the line voltages v_{AB} and v_{BC} under the ITSC fault. However, if the "circulant" characteristic of branch inductance matrices (see appendix A of [11]), and the constraint of branch currents are considered, adding all circuit branch voltage equations will give

$$
v_A + v_B + v_C = (e_A + e_B + e_C)
$$
$$
- \frac{1}{n} \left[R_{A1f} i_f + \left(\sum_{k=1}^{n} \left(\mathbf{M}_{Af} + \mathbf{M}_{Bf} + \mathbf{M}_{Cf} \right)_k \right) \frac{di_f}{dt} \right]
$$

$$(5)$$

where e_B and e_C are branch back-EMFs of phase B and C, respectively. $\left(\mathbf{M}_{Af} + \mathbf{M}_{Bf} + \mathbf{M}_{Cf}\right)_k$ indicates the kth element of the sum of $\mathbf{M}_{Af}$, $\mathbf{M}_{Bf}$, and $\mathbf{M}_{Cf}$. It is worth mentioning that all branch-to-neutral voltages of the same phase are equal, and this is the same for the branch back-EMFs.

When the sum of the three branch-to-neutral voltages in Equation (5) is known, the two line voltages v_{AB} and v_{BC} can be expressed as

$$\begin{cases} v_{AB} = v_A - v_B \\ v_{BC} = v_B - v_C = v_A + 2v_B - (v_A + v_B + v_C) \end{cases} \quad (6)$$

The use of Equations (5) and (6) will yield the three phase voltages from the line voltages. Once the branch currents in all circuit branches are known, the electromagnetic torque under ITSC faults can be expressed as

$$T_e = \frac{(\mathbf{e}_A)^T \mathbf{i}_A + (\mathbf{e}_B)^T \mathbf{i}_B + (\mathbf{e}_C)^T \mathbf{i}_C - e_{A1f} i_f}{\omega_{rm}} + T_{cog} \quad (7)$$

where ω_{rm} is the rotor mechanical speed (rad/s) and T_{cog} is the cogging torque which can be calculated using FE models.

From the above model equations, it is evident that the level of complexity of the established fault model using branch currents as state variables is determined by the number of parallel branches. Generally speaking, the larger the number of parallel branches, the larger the number of first-order differential equations must be used to describe the faulty machine behaviours, thus more efforts are required to build the fault model. In fact, the number of first-order differential equations of the complete model to predict the machine behaviour under ITSC fault is $3n + 2$ for the studied SPM machines with n parallel branches in every phase. Therefore, it would be much better if the number of state variables especially the number of derivatives of state variables in every differential equation is minimised as this will significantly simplify the fault model. To this end, multiphase Clarke transformation is adopted in Section 4, which can considerably reduce the model complexity.

3 | INDUCTANCE CALCULATION

It can be seen from Section 2 that all elements in the nine branch inductance matrices and three fault inductance vectors need to be known while building the fault models in Matlab/Simulink. Therefore, this section will be dedicated to the theoretical calculation of inductances using an analytical method, which will also be validated by 2D FE modelling (using JMAG software package). To be consistent with the analytical modelling, the 2D FE modelling also neglects the core saturation.

3.1 | Calculation of inductances

It has been mentioned that in [10, 11], there are three components in the phase self- and mutual- inductances such as

$$\begin{cases} L_{ph} = L_g + L_{slot} + L_{end} \\ M_{ph} = M_g + M_{slot} + M_{end} \end{cases} \quad (8)$$

where the airgap components L_g, M_g corresponds to the flux traversing the airgap, the slot-leakage components L_{slot}, M_{slot} are the leakage fluxes crossing the slots, and the end-turn leakage components L_{end} and M_{end} are associated with the leakage fluxes in the end-winding region. In this paper, the end-turn leakage components are neglected for simplicity and initial study.

As mentioned previously, the airgap inductance components could be determined by the WFA detailed in [11, 22]. If the branch A1 in Figure 2 has an ITSC fault, the branch A1 will be separated into two parts: the faulty turns (A11_fm) and the remaining healthy turns (A11_hb, A11_ht, and A1_hc).

After the winding functions of the remaining healthy turns, the faulty turns in the faulty branch and other branches are derived, all elements of the branch inductance matrices can be calculated using the WFA together with the slot permeance method as detailed in [10, 11]. It is also found that all branch inductance matrices are circulant matrices (see appendix A of [11]). According to the characteristics of the circulant matrices, once the elements in the first row are known, all the elements of the circulant matrices can be determined accordingly. As a result, all the inductances needed for the fault modelling can be obtained as

$$\begin{cases} L_{A1A1} = L_{B1B1} = L_{C1C1} = L_1 \\ M_{A1Aj} = M_{B1Bj} = M_{C1Cj} = M_1 \ (j = 2, 3, \cdots, n) \\ M_{A1B1} = M_{B1C1} = M_2 \\ M_{A1Bj} = M_{B1Cj} = M_1 \ (j = 2, 3, \cdots, n) \\ M_{A1Cj} = M_1 \ (j = 2, 3, \cdots, n-1) \\ M_{A1C1} = M_1 + M_\alpha \\ M_{A1Cn} = M_1 + M_\beta \end{cases} \quad (9)$$

with

$$\begin{cases} L_1 = \frac{\mu_0 r_e l_e}{g_e} \frac{r(2p-r)}{2p^2} \pi (n_c)^2 + 2r(n_c)^2 \mu_0 l_e \left[\frac{h_s}{3S_\omega}\right] \\ M_1 = \frac{\mu_0 r_e l_e}{g_e} \left(-\frac{r^2}{2p^2}\right) \pi (n_c)^2 \text{ and } M_2 = -\frac{(2p-3r)}{3r} M_1 \\ M_\beta = \frac{\mu_0 r_e l_e}{g_e} \frac{1}{3p} \pi (n_c)^2 \text{ and } \quad M_\alpha = (r-1)M_\beta \end{cases}$$
$$(10)$$

where the meanings of μ_0, r_e, l_e, g_e, h_s, S_ω and p are the same as those in [11].

As for the elements in the fault inductance vectors, they are given as

$$\begin{cases} L_{A1f,A1f} + M_{A1b,A1f} = L_{11} \quad M_{B1,A1f} = M_{Cn,A1f} = M_{22} \\ M_{Aj,A1f} = M_{Bj,A1f} = M_{11} \ (j = 2, 3, \cdots, n) \\ M_{Cj,A1f} = M_{11} \ (j = 1, 2, \cdots, n-1) \end{cases}$$

$$(11)$$

Regarding $L_{A1f,A1f}$ and $M_{A1b,A1f}$, the airgap and slot-leakage inductance components (indicated by subscripts "g" and "slot", respectively) will be calculated separately as follows

$$L_{11} = L_{A1f,A1f} + M_{A1b,A1f} = (L_{A1f,A1f})_g + (L_{A1f,A1f})_{slot} \\ + (M_{A1b,A1f})_g + (M_{A1b,A1f})_{slot}$$

$$(12)$$

with

$$(L_{A1f,A1f})_g + (M_{A1b,A1f})_g = \frac{\mu_0 r_e l_e}{g_e} \frac{(2p-r)}{2p^2} \mu_1 \pi (n_c)^2 \quad (13)$$

$$(L_{A1f,A1f})_{slot} = 2\mu_0 l_e \left(\frac{n_c}{h_s}\right)^2 \frac{(h_b - h_a)^2}{S_\omega} \left(h_s - \frac{1}{3}h_a - \frac{2}{3}h_b\right)$$

$$(14)$$

$$(M_{A1b,A1f})_{slot} = 2\mu_0 l_e \left(\frac{n_c}{h_s}\right)^2 \left[\frac{h_a(h_b - h_a)^2}{2S_\omega} \right. \\ \left. + \frac{(h_b - h_a)}{2S_\omega} \left\{(h_s - h_b + h_a)^2 - h_a^2\right\}\right]$$

$$(15)$$

where h_a and h_b represent the fault locations along the slot, the same as those in [11].

In addition, M_{22} and M_{11} in Equation (11) can be expressed as

$$M_{11} = -\frac{\mu_0 r_e l_e}{g_e} \frac{r}{2p^2} \mu_1 \pi (n_c)^2 \quad \text{and} \quad M_{22} = \frac{(3r - 2p)}{3r} M_{11} \quad (16)$$

Equations (10) to (16) show that the inductance elements in all branch inductance matrices and corresponding fault inductance vectors can be easily updated if the series-parallel coil connection $rS \times nP$ of a SPM machine is changed. This means that the developed fault model in this paper is generic and can be applicable to SPM machines with different series-parallel coil connections.

3.2 | Results of inductance calculations

3.2.1 | Elements of branch inductance matrices

The key parameters of the studied 3kW SPM machine are listed in Table 1. This machine is the same as the one investigated in [10, 11], except this machine adopts different combinations of series-parallel-connected coils rather than series-connected or parallel-connected coils.

By the way of example, the 2D FE linear inductances of the 3kW machine with 2S × 8P coil connection are shown in Figure 3a. In Figure 3b, the relative error of the inductances is the difference between the 2D analytical and FE inductances divided by the corresponding 2D FE inductances.

It is worth mentioning that, although all three series-parallel coil connections have been investigated, only the

TABLE 1 Specifications of the studied 3kW surface-mounted permanent magnet (SPM) machine.

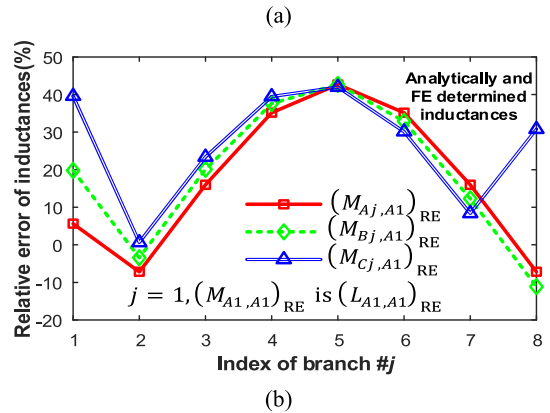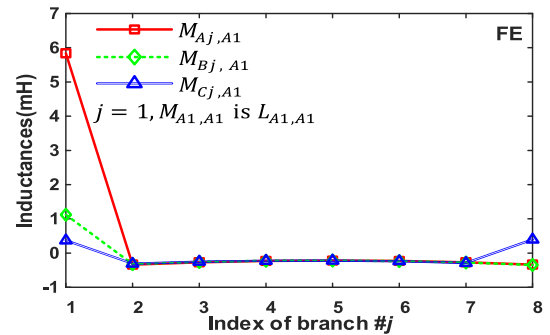|	Series-parallel coil connections (rS × nP)		
	8S × 2P	4S × 4P	2S × 8P
Rated power (kW)		3	
Rated speed (rpm)		170	
Rated voltage (Vrms)	345	172.5	86.3
Phase current (Arms)	5	10	20
Series turns/coil		52	
Numbers of slots/poles		96/32	
Rotor outer diameter (mm)		426.4	
Stack length (mm)		110	
Airgap length (mm)		2	

(a)

(b)

FIGURE 3 Characteristics of inductances between #A1 branch and other branches. (a) 2D FE results and (b) relative errors between analytical and FE results.

results for 2S $\times$ 8P coil connection are shown due to space limitation. In addition, to be consistent with the conditions used by the analytical method, all permanent magnets in the FE model are treated as air, and the stator and rotor cores are assumed to be magnetically linear with a relative permeability $\mu_r = 10000$. After setting these conditions for materials, 1A DC current is then supplied to only the A1 branch, meaning all other branches in the three phases are open-circuited.

Due to the symmetrical 3-phase overlapping windings adopted by the studied SPM machine, the branch inductance matrices $\mathbf{L}_{AA} = \mathbf{L}_{BB} = \mathbf{L}_{CC}$ and $\mathbf{M}_{AB} = \mathbf{M}_{BC}$. As mentioned earlier, the determination of elements in the first row of all these branch inductance matrices will be enough to determine all the elements of these matrices. Hence showing the characteristics of inductances only related to the A1 branch is sufficient.

Although there are some large errors between analytical and FE inductances in Figure 3b, due to the small values of these inductances, they may not have a significant impact on the accuracy of the developed fault model, as it will be investigated in Section 5.

3.2.2 | Equivalent phase inductances

Further calculations of the equivalent phase self- and mutual inductances for the 2S $\times$ 8P coil connection have been carried out, and the results are shown in Table 2. It is worth noting that how to calculate the equivalent phase self- and mutual-inductances for 3-phase windings with series-parallel coil connections will be left in Section 4. From Table 2, much smaller differences in the equivalent phase self- and mutual inductances can be observed. This means that the predicted phase currents of the healthy machines by the analytical and linear FE models would be very much similar. As for the inductance values and relative errors of inductances between the short-circuited turns and other branches, they are very much similar to those shown in Figure 3 and hence are not presented here to avoid duplication.

4 | MODEL SIMPLIFICATION

Although the proposed fault model uses branch currents as state variables in the direct phase domain, it does not provide much meaningful physical insights because all the elements in the branch inductance matrices would not be zeros in theory, making the analyses very complicated and the computation

TABLE 2 Equivalent phase self- and mutual-inductances (mH).

	L_{AA}	M_{AB}	M_{AC}
2D FE	0.495	−0.0953	−0.0953
Analytical	0.499	−0.104	−0.104
Relative error (%)	0.9	8.9	8.9

quite intensive. Meanwhile, it is difficult to construct a fault model in the Matlab/Simulink if the number of parallel branches n is large ($n \geq 10$), which is very often the case for large-power wind generators. To simplify the fault model, that is, to make all the branch inductance matrices sparse ones, in this paper, the original branch currents, voltages, and back-EMFs are transformed into new variables using the multiphase Clarke transformation matrix $\boldsymbol{C}$ of [11] (see appendix B of [11]). The number of parallel branches n will replace the number of pole pairs p appearing in $\boldsymbol{C}$ of [11] to keep matrix dimensions consistent) such as

$$\begin{bmatrix} \mathbf{f}'_A \\ \mathbf{f}'_B \\ \mathbf{f}'_C \end{bmatrix} = \begin{bmatrix} \boldsymbol{C} & \mathbf{0} & \mathbf{0} \\ \mathbf{0} & \boldsymbol{C} & \mathbf{0} \\ \mathbf{0} & \mathbf{0} & \boldsymbol{C} \end{bmatrix} \begin{bmatrix} \mathbf{f}_A \\ \mathbf{f}_B \\ \mathbf{f}_C \end{bmatrix} \tag{17}$$

where $\mathbf{f}'_A$, $\mathbf{f}'_B$ and $\mathbf{f}'_C$ are the corresponding transformed branch current, voltage, and back EMF vectors. In this paper, $\boldsymbol{C}$ has the power invariant form, that is, $\boldsymbol{C}^{-1} = \boldsymbol{C}^T$. Therefore, it is quite easy to obtain $\mathbf{f}_A$, $\mathbf{f}_B$ and $\mathbf{f}_C$ from $\mathbf{f}'_A$, $\mathbf{f}'_B$ and $\mathbf{f}'_C$ such as

$$\begin{aligned} \begin{bmatrix} \mathbf{f}_A \\ \mathbf{f}_B \\ \mathbf{f}_C \end{bmatrix} &= \begin{bmatrix} \boldsymbol{C}^{-1} & \mathbf{0} & \mathbf{0} \\ \mathbf{0} & \boldsymbol{C}^{-1} & \mathbf{0} \\ \mathbf{0} & \mathbf{0} & \boldsymbol{C}^{-1} \end{bmatrix} \begin{bmatrix} \mathbf{f}'_A \\ \mathbf{f}'_B \\ \mathbf{f}'_C \end{bmatrix} \\ &= \begin{bmatrix} \boldsymbol{C}^T & \mathbf{0} & \mathbf{0} \\ \mathbf{0} & \boldsymbol{C}^T & \mathbf{0} \\ \mathbf{0} & \mathbf{0} & \boldsymbol{C}^T \end{bmatrix} \begin{bmatrix} \mathbf{f}'_A \\ \mathbf{f}'_B \\ \mathbf{f}'_C \end{bmatrix} \end{aligned} \tag{18}$$

After using the multiphase Clarke transformation, the new circuit-branch voltage equations can be expressed as

$$\begin{aligned} \begin{bmatrix} \mathbf{v}'_A \\ \mathbf{v}'_B \\ \mathbf{v}'_C \end{bmatrix} &= \begin{bmatrix} \mathbf{L}'_{AA} & \mathbf{M}'_{AB} & \mathbf{M}'_{AC} \\ \mathbf{M}'_{BA} & \mathbf{L}'_{BB} & \mathbf{M}'_{BC} \\ \mathbf{M}'_{CA} & \mathbf{M}'_{CB} & \mathbf{L}'_{CC} \end{bmatrix} \frac{\mathrm{d}}{\mathrm{d}t} \begin{bmatrix} \mathbf{i}'_A \\ \mathbf{i}'_B \\ \mathbf{i}'_C \end{bmatrix} + R_{\mathrm{cb}} \begin{bmatrix} \mathbf{i}'_A \\ \mathbf{i}'_B \\ \mathbf{i}'_C \end{bmatrix} \\ &+ \begin{bmatrix} \boldsymbol{e}'_A \\ \boldsymbol{e}'_B \\ \boldsymbol{e}'_C \end{bmatrix} - \begin{bmatrix} \boldsymbol{C} & \mathbf{0} & \mathbf{0} \\ \mathbf{0} & \boldsymbol{C} & \mathbf{0} \\ \mathbf{0} & \mathbf{0} & \boldsymbol{C} \end{bmatrix} \\ &\times \left(\begin{bmatrix} R_{A1f} \\ 0 \\ \vdots \\ 0 \end{bmatrix} i_f + \begin{bmatrix} \boldsymbol{M}_{Af} \\ \boldsymbol{M}_{Bf} \\ \boldsymbol{M}_{Cf} \end{bmatrix} \frac{\mathrm{d}i_f}{\mathrm{d}t} \right) \end{aligned} \tag{19}$$

where $\mathbf{L}'_{xx} = \boldsymbol{C}\mathbf{L}_{xx}\boldsymbol{C}^T$, $\mathbf{M}'_{xy} = \boldsymbol{C}\mathbf{M}_{xy}\boldsymbol{C}^T$. "$x$" and "$y$" represent different phases amongst A, B, and C. If the inductances calculated by analytical method are employed in this analytical model, then $\mathbf{L}'_{xx}$, $\mathbf{M}'_{AB}$, and $\mathbf{M}'_{BC}$ are diagonal matrices and $\mathbf{M}'_{AC}$ is a block diagonal matrix.

To sum up, after the transformation, the fault model is greatly reduced because the number of the first-order

derivatives of state variables in every circuit branch voltage equation is reduced from $3n + 1$ to the minimum value. To be more specific, there will only be 3 to 5 derivatives of state variables after the transformation.

The transformed voltage equation for the short-circuited path will be

$$\left(R_f + R_{A1f}\right)i_f + L_{A1f,A1f}\frac{di_f}{dt} - e_{A1f} - R_{A1f}\left(\mathbf{C}^T\mathbf{i}'_A\right)_1$$
$$= \left(\mathbf{CM}_{Af}\right)^T\frac{d\mathbf{i}'_A}{dt} + \left(\mathbf{CM}_{Bf}\right)^T\frac{d\mathbf{i}'_B}{dt} + \left(\mathbf{CM}_{Cf}\right)^T\frac{d\mathbf{i}'_C}{dt} \quad (20)$$

where $\left(\mathbf{C}^T\mathbf{i}'_A\right)_1$ is the first element of the vector $\mathbf{C}^T\mathbf{i}'_A$. The torque equation now can be expressed as

$$T_e = \frac{\left(e_A i_A + e_B i_B + e_C i_C - e_{A1f} i_f\right)}{\omega_{rm}} + T_{cog} \quad (21)$$

It should be mentioned that during the simplification process, the relationship between the phase self- and mutual-inductances for 3-phase windings having series-parallel-connected coils (L_{SP} and M_{SP}) and those having the series-connected coils (L_S and M_S) can be derived such as

$$\begin{cases} \left(L_{xx}\right)_{SP} = \frac{1}{n}\sum_{j=1}^{n}\left(\mathbf{L}_{xx}\right)_{1j} = \frac{1}{n^2}\left(L_{xx}\right)_S \\ \\ \left(M_{xy}\right)_{SP} = \frac{1}{n}\sum_{j=1}^{n}\left(\mathbf{M}_{xy}\right)_{1j} = \frac{1}{n^2}\left(M_{xy}\right)_S \end{cases} \quad (22)$$

5 | SIMULATION RESULTS

As can be seen from Figure 2 in the FE simulations, the studied 3kW SPM machine is excited with 3-phase balanced sinusoidal voltages. In addition, the machine's rotor mechanical speed is kept constant during the whole operation period to shorten the simulation time. It is also worth mentioning that FE and Matlab/Simulink simulations for this 3kW SPM machine with different coil configurations such as 8S × 2P, 4S × 4P and 2S × 8P have been carried out under different fault severities and different speeds. It is found that all the FE and analytical results generally have good agreements. However, due to space limitation, only some representative results are provided in this section.

5.1 | One coil short-circuited (2S × 8P)

Figure 4 shows a comparison of some branch currents in all three phases before and after the one-coil short-circuit fault. It can be seen from Figure 4a that the branch currents obtained by these two models match well. It is worth noting that i_{A3} to i_{A8} are very much similar to i_{A2}, i_{B3} to i_{B7} are very much similar to i_{B2}, and i_{C3} to i_{C7} are very much similar to i_{C2}.
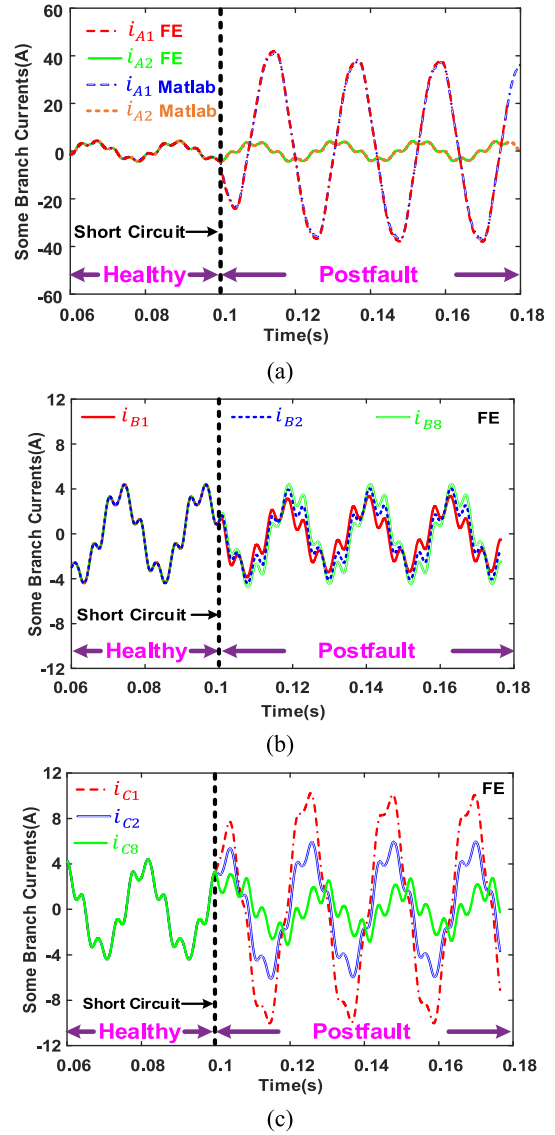

FIGURE 4 Some branch currents of three phases before and after one-coil short-circuit fault. (a) phase A, (b) phase B, and (c) phase C.

Hence they are not shown in these figures. Figure 4b,c show some branch currents of phases B and C. Here only the FE results are used, as they are very much the same as the analytical results. It is found that, different from the assumption made in [15, 16], the branch currents of the remaining healthy phases especially phase C are unequal for this integer-slot SPM machine after the ITSC fault.

In addition, it is found that the sum of i_{C1} and i_{Cn} is about 2 times as large as i_{C2} for 4S × 4P and 2S × 8P coil connections. This means that more assumptions can be made to greatly reduce the number of differential equations in the fault model if some loss in the model accuracy is allowed. This may be very useful for developing fault mitigation strategies. Meanwhile, the currents in the short-circuited coil predicted by the two models are shown in Figure 5. It can be seen that there is a significant increase in the current of the short-circuited coil. For example, the amplitude of current in the short-

circuited coil increases from 4.25 to 38.6A after the ITSC fault. This will lead to changes in the phase current, and hence changes in the developed electromagnetic torque, as shown in Figure 6.

It is worth noting that, in Figure 6, the cogging torque has already been included in the analytical model according to (7) or (21) to give more accurate prediction of torque ripple under the ITSC fault. It can be observed that after the ITSC fault, the torque ripple increases only slightly. This is mainly because each phase current is the sum of 8 individual branch currents. As a result, although some branch currents change significantly, the phase current is only slightly affected.

5.2 | Different fault severities

The amplitudes of inter-turn short-circuit currents obtained by the FE and Matlab/Simulink simulations for the 3kW SPM machine with different coil connections such as 8S × 2P, 4S × 4P, and 2S × 8P and under different fault severities are shown in Figure 7. Here, the fault location is at the bottom of the slot, that is, $h_a = h_s/n_c$. A generally good agreement between the FE and analytical results can also be observed. The slightly larger difference between FE and Matlab/Simulink results for 8S × 2P and 4S × 4P coil connections is mainly because the relative errors between the inductances obtained
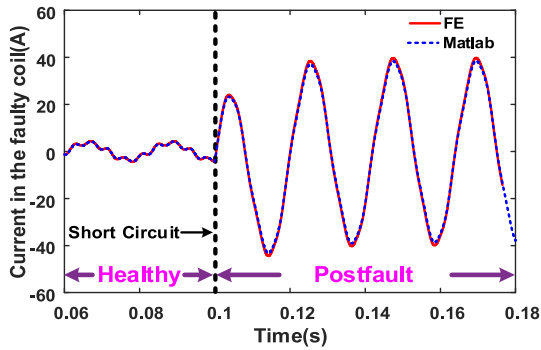
by linear 2D FE and analytical approaches are larger when the number of branches is smaller.

It is also found that when the coil faulty turns ratio increases, the ITSC current reduces. This is the case for all series-parallel coil connections. The reason for this is that the ITSC current is mainly determined by the ratio of open-circuit flux linkage of the short-circuited turns to their self-inductance. When the faulty turns ratio increases, the self-inductance of the short-circuited turns (proportional to number of turns squared) increases faster than its open-circuit flux linkage (proportional to number of turns). In addition, if the coil faulty turns ratio is the same, different series-parallel coil connections will have negligible influence on the amplitude of the ITSC current. This means that the impact of the ITSC faults on all series-parallel coil connections is the same.

6 | EXPERIMENTAL VALIDATIONS

6.1 | Test rig setup

A small-scale 24-slot 8-pole SPM machine prototype has been manufactured to validate the proposed fault model. The main parameters of this prototype are listed in Table 3. The test rig setup of this prototype is shown in Figure 8. As this prototype has single-layer, full-pitch and distributed winding structure, each phase will have 4 coils in total. To achieve a series-parallel coil connection, each phase winding will have 2 parallel branches and each branch has 2 coils connected in series.

In addition, it is worth mentioning that all the faults are introduced in the A11 coil and three fault scenarios can be carried out, that is, one-coil, half-a-coil, and single-turn short-

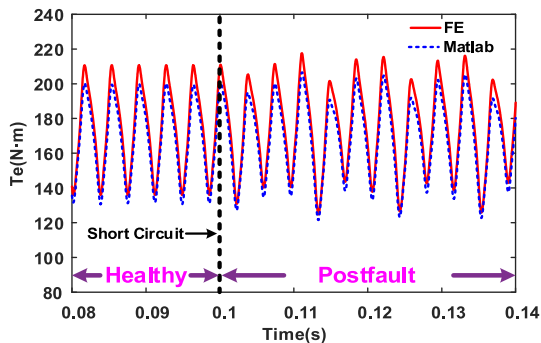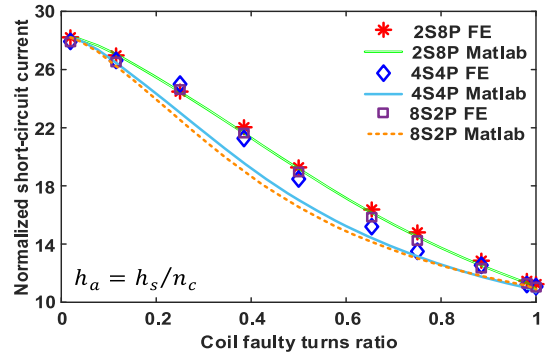**FIGURE 5** Currents in the short-circuited coil under the one-coil short-circuit fault.

FIGURE 6 Change in on-load torque of the 3kW surface-mounted permanent magnet (SPM) machine before and after the one coil short-circuit fault.

FIGURE 7 Amplitudes of ITSC current versus coil faulty turns ratio for different series-parallel coil connections.

TABLE 3 Specifications of 24-slot 8-pole surface-mounted permanent magnet (SPM) prototype machine.

Rated torque (Nm)	1.09	Stator outer diameter (mm)	100
Rated current rms (A)	2.5	Rotor outer diameter (mm)	49
Series turns/coil	20	Air gap length (mm)	1
Slots/poles	24/8	Stack length (mm)	50

circuit faults. The SPM machine in Figure 8 is used as a generator driven by a DC machine, and its 3-phase terminals are connected to a 3-phase rheostat, which replaces the 3-phase voltage sources in Figure 2. In this way the hardware implementation becomes much simpler but the main purpose such as fault model validation can still be achieved.

Meanwhile, it is found that it is sufficient to use the Magtrol Model 3401 torque display instead of a position encoder to record the speed information, which is an input to the analytical model built in Matlab/Simulink. This is because the 2.2kW dc machine has a good torque-speed characteristic to reduce the speed ripple caused by the 150W 24-slot 8-pole SPM machine prototype, which acts as its load.

6.2 | Inductances

The analytical and 2D linear FE inductances have been calculated first, and a good agreement between them can be observed, as shown in Table 4. To consider the influence of core saturation and long end windings on inductance values, a nonlinear 3D FE model of this prototype has also been built using JMAG, and the inductance results are compared against the measured ones by using the Hioki IM3533-01 LCR Metre. The nonlinear 3D FE and measured inductances are listed in Table 5. It can be seen from Table 5 that all the relative errors between the nonlinear 3D FE and measured inductances are generally acceptable.

As for the nonlinear 3D FE and measured inductances related to the short-circuited turns, especially those associated with the single turn short-circuit fault, they can be estimated by using the inductances related to coil A11. For example, the self-inductance is proportional to the square of the number of turns in a coil, and the mutual inductance is proportional to the number of turns. As such, all inductances will be known for the three fault scenarios.

6.3 | Branch and faulty currents under half-a-coil short- circuit fault

To validate the proposed fault model, all the three fault scenarios (single-turn, half-a-coil, and one-coil short-circuit faults) have been carried out under different speeds and loads. It is found that the measured and simulated results generally match well. However, due to page limit, only some representative results of half-a-coil short-circuit fault are presented.

The measured and predicted branch currents and phase currents at about 900rpm with a resistive load of 1.2Ω are shown in Figures 9 and 10, respectively. It is worth mentioning that the simulated branch and phase currents by using 3D nonlinear FE and measured inductances in the fault model are very much similar. Therefore, for more clarity, only the

TABLE 5 3D FE and measured inductances (µH) of the machine prototype.

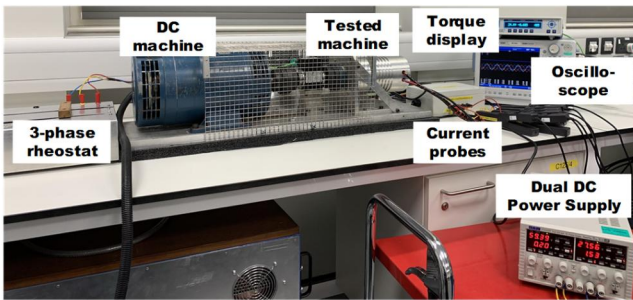| Method	L_{A1A1}	M_{A1A2}	M_{A1B1}	M_{A1B2}
3D FE (nonlinear)	316.8	−25.8	−14.5	−34.1
Measured	317.5	−27.45	−13.68	−35.3
Difference (%)	−0.22	−6.4	5.65	−3.52

FIGURE 8 Test rig setup.

TABLE 4 2D FE and analytical inductances (µH) of the machine prototype.

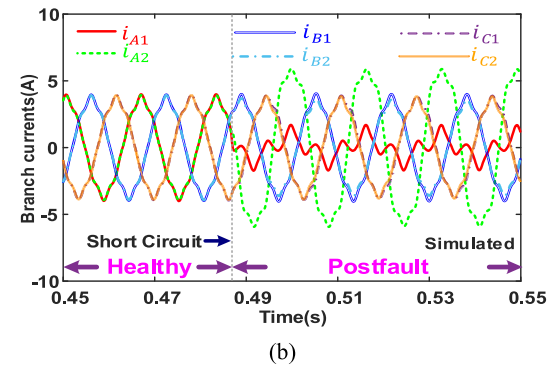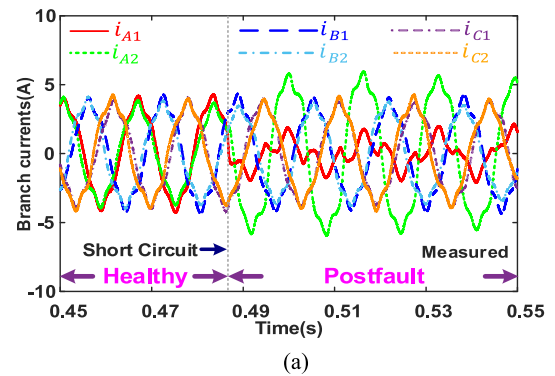| Method	L_{A1A1}	M_{A1A2}	M_{A1B1}	M_{A1B2}
2D FE (linear)	331.7	−59.4	19.3	−59.5
2D analytical	283.5	−63.1	21	−63.1
Difference (%)	14.53	−6.23	−8.81	−6.05

FIGURE 9 Branch currents before and after half-a-coil short-circuit fault. (a) Measured and (b) predicted.

simulated results using measured inductances have been provided in Figures 9 and 10.

Like the branch currents and phase currents, the difference between the simulated i_{A1f} using the 3D nonlinear FE and directly measured inductances is very small, as shown in Figure 11. In addition, although there is a slight discrepancy between the measured and simulated i_{A1f}, it is still within the acceptable range.

6.4 | Different loads and speeds

To further validate the fault model, more tests at different loads and speeds under the half-a-coil short-circuit fault have also been carried out, and the results are shown in Figure 12. It can be seen that the measured currents (amplitude) in the short-circuited turns A11_fm and faulty phase A with two different resistive loads (no-load and 1.2Ω) and different rotor speeds match well with the simulations. Therefore, together with other results in the previous sections, the accuracy of the proposed fault model can be validated.

It should be mentioned that in Section 4, the effectiveness of the developed fault model and model simplification method have been fully validated by the 2D FE and Simulink simulation results when analytical inductances are used. However, in this section, only the fault model with nonlinear inductances has been validated. In our future work whether the model simplification method can be applied to the developed fault
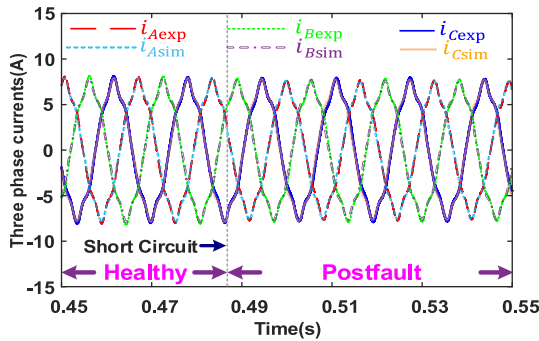
model with nonlinear inductances will be studied. If this succeeds, then the fault model and model simplification method may be easily extended to other types of non-PM machines and also their multiphase counterparts with practical winding configurations. This is particularly useful for large-power electrical machines, in which the prediction of changes in machine currents and voltages under ITSC faults is very difficult due to their complex winding configurations.

7 | CONCLUSION

This paper develops a general and simple analytical model in a concise block matrix form for PM wind generators with different series-parallel coil connections under inter-turn short-circuit (ITSC) fault. The fault model is divided into two parts, that is, the healthy part of the machine model uses branch currents as state variables and the faulty part is represented by the current in the external short-circuited path and the inductances between the short-circuited turns and every branch windings. In the fault model, inductances for different series-parallel coil connections have been calculated by an analytical method such as WFA together with slot permeance method. Based on the characteristics of the calculated inductances and the concise block matrix form of the developed fault model, the multiphase Clarke transformation has been proposed to simplify the fault model. This simplification not only significantly lowers the modelling complexity, but also reduces the computational burden considerably, especially for large-power SPM wind generators under ITSC faults. In the process of model simplification, the healthy machine model using branch currents as state variables have proven to be equivalent to that using 3-phase currents as state variables. Simulation results from 2D FE and analytical models generally match well for different fault scenarios and different coil connections. This validates the accuracy of the proposed fault model and model simplification method when analytical inductances are used. The analytical fault model proposed in this paper can be very useful for developing model-based fault detection and mitigation strategies for large wind power generators. For these machines, modelling methods like the FE or magnetic

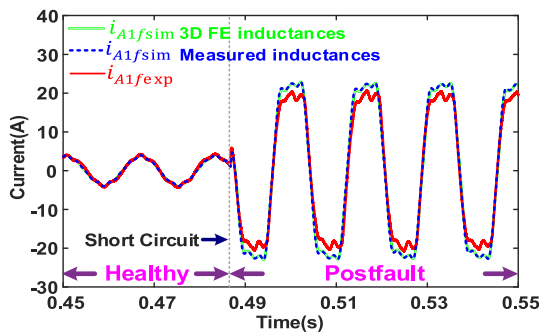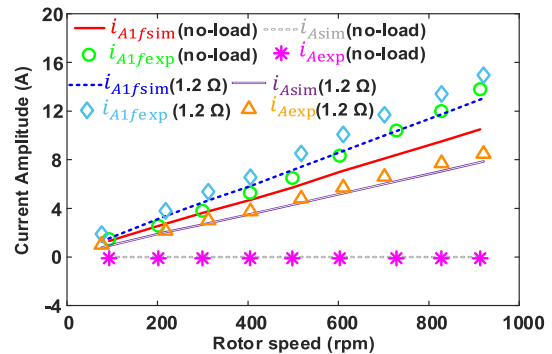**FIGURE 10** Measured and predicted 3-phase currents before and after half-a-coil short-circuit fault.

FIGURE 11 Measured and predicted fault currents (i_{A1f}) in the short-circuited turns before and after half-a-coil short-circuit fault.

FIGURE 12 Amplitudes of current of short-circuited turns and faulty phase under different resistive loads and speeds.

equivalent circuit can be very time-consuming and performing fault tests may be difficult. From the developed fault model, it is found that the branch currents of the remaining healthy phases under ITSC fault are not always equal and different series-parallel coil connections have negligible influence on the amplitude of ITSC current at the same torque and speed. Finally, the proposed fault model is further validated by a series of experiments on a 24-slot 8-pole machine prototype.

AUTHOR CONTRIBUTIONS

Zeting Mei: Writing—original draft, Visualisation, Investigation, Validation, Methodology, Formal analysis, Conceptualisation. **Guang-Jin Li**: Supervision, Writing—review & editing. **Zi-Qiang Zhu**: Funding acquisition, Writing—review & editing. **Richard Clark**: Funding acquisition, Resources, Project administration, Writing—review & editing. **Arwyn Thomas**: Funding acquisition, Resources. **Ziad Azar**: Funding acquisition, Resources.

CONFLICT OF INTEREST STATEMENT

The authors declare no conflict of interest.

DATA AVAILABILITY STATEMENT

Data subject to third party restrictions.

ORCID

Guang-jin Li https://orcid.org/0000-0002-5956-4033
Zi-Qiang Zhu https://orcid.org/0000-0001-7175-3307

REFERENCES

1. Yaramasu, V., et al.: High-power wind energy conversion systems: state-of-the-art and emerging technologies. Proc. IEEE 103(5), 740–788 (2015). https://doi.org/10.1109/jproc.2014.2378692
2. Freire, N.M.A., Marques Cardoso Antonio, J.: Fault detection and condition monitoring of PMSGs in offshore wind turbines. Machines 9(11), 260 (2021). https://doi.org/10.3390/machines9110260
3. Ribrant, J., Bertling, L.M.: Survey of failures in wind power systems with focus on Swedish wind power plants during 1997-2005. IEEE Trans. Energy Convers. 22(1), 167–173 (2007). https://doi.org/10.1109/tec.2006.889614
4. Nandi, S., Toliyat, H.A., Li, X.: Condition monitoring and fault diagnosis of electrical motors – a review. IEEE Trans. Energy Convers. 20(4), 719–729 (2005). https://doi.org/10.1109/tec.2005.847955
5. Alewine, K., Chen, W.: A review of electrical winding failures in wind turbine generators. IEEE Electr. Insul. Mag. 28(4), 8–13 (2012). https://doi.org/10.1109/mei.2012.6232004
6. Bonnett, A.H., Soukup, G.C.: Cause and analysis of stator and rotor failures in three-phase squirrel-cage induction motors. IEEE Trans. Ind. Appl. 28(4), 921–937 (1992). https://doi.org/10.1109/28.148460
7. Orlowska-Kowalska, T., et al.: Fault diagnosis and fault-tolerant control of PMSM Drives-state of the art and future challenges. IEEE Access 10, 59979–60024 (2022). https://doi.org/10.1109/access.2022.3180153

8. Moon, S., et al.: Interturn short fault diagnosis in a PMSM by voltage and current residual analysis with the faulty winding model. IEEE Trans. Energy Convers. 33(1), 190–198 (2018). https://doi.org/10.1109/tec.2017.2726142
9. Fonseca, D.S.B., Santos, C.M.C., Cardoso, A.J.M.: Stator faults modeling and diagnostics of line-start permanent magnet synchronous motors. IEEE Trans. Ind. Appl. 56(3), 2590–2599 (2020). https://doi.org/10.1109/tia.2020.2979674
10. Mei, Z., et al.: Scaling effect on inter-turn short-circuit fault of PM machines for wind power application. IEEE Trans. Ind. Appl., 1–11 (2022)
11. Mei, Z.T., et al.: Modelling and analysis of inter-turn short-circuit fault of PM Machines with parallel-connected coils. IEEE Trans. Energy Convers., 1–11 (2023). https://doi.org/10.1109/tec.2023.3234332
12. Wang, X.H., et al.: Transient behaviour of salient-pole synchronous machines with internal stator winding faults. IEE Proc. Elec. Power Appl. 149(2), 143–151 (2002). https://doi.org/10.1049/ip-epa:20020068
13. Tu, X., et al.: A new model of synchronous machine internal faults based on winding distribution. IEEE Trans. Ind. Electron. 53(6), 1818–1828 (2006). https://doi.org/10.1109/tie.2006.885125
14. Tu, X., et al.: Modeling and real-time simulation of internal faults in synchronous generators with parallel-connected windings. IEEE Trans. Ind. Electron. 54(3), 1400–1409 (2007). https://doi.org/10.1109/tie.2007.892004
15. Gu, B., Choi, J., Jung, I.: Development and analysis of interturn short fault model of PMSMs with series and parallel winding connections. IEEE Trans. Power Electron. 29(4), 2016–2026 (2014). https://doi.org/10.1109/tpel.2013.2265400
16. Qian, H., Guo, H., Ding, X.: Modeling and analysis of interturn short fault in permanent magnet synchronous motors with multistrands windings. IEEE Trans. Power Electron. 31(3), 2496–2509 (2016). https://doi.org/10.1109/tpel.2015.2439574
17. Naderi, P.: Magnetic-equivalent-circuit approach for inter-turn and demagnetisation faults analysis in surface mounted permanent-magnet synchronous machines using pole specific search-coil technique. IET Electr. Power Appl. 12(7), 916–928 (2018). https://doi.org/10.1049/iet-epa.2017.0403
18. Forstner, G., Kugi, A., Kemmetmüller, W.: A magnetic equivalent circuit based modeling framework for electric motors applied to a PMSM with winding short circuit. IEEE Trans. Power Electron. 35(11), 12285–12295 (2020). https://doi.org/10.1109/tpel.2020.2986042
19. Dallas, S.E., Safacas, A.N., Kappatou, J.C.: Interturn stator faults analysis of a 200-MVA hydrogenerator during transient operation using FEM. IEEE Trans. Energy Convers. 26(4), 1151–1160 (2011). https://doi.org/10.1109/tec.2011.2166401
20. Ge, B., et al.: Improved model of synchronous generators internal faults based on circuit-coupled FEM. IEEE Trans. Energy Convers. 32(3), 876–884 (2017). https://doi.org/10.1109/tec.2017.2694883
21. Gao, C., et al.: Research on interturn short-circuit fault indicators for direct-drive permanent magnet synchronous motor. IEEE J. Emerg. Sel. Top. Power Electron. 10(2), 1902–1914 (2022). https://doi.org/10.1109/jestpe.2021.3059287
22. Lipo, T.A.: Analysis of Synchronous Machines, 2nd ed. CRC Press (2012)

How to cite this article: Mei, Z., et al.: In-depth investigation of inter-turn short-circuit faults of surface-mounted permanent magnet machines with series-parallel coil connections. IET Electr. Power Appl. 1–11 (2023). https://doi.org/10.1049/elp2.12326